Stretching and Curvature of Material Lines in Chaotic Flows

Jean-Luc Thiffeault[*]

Department of Applied Physics and Applied Mathematics,
Columbia University, New York, NY 10027[†]
(Dated: October 29, 2018)

As a streak of dye is advected by a chaotic flow, it stretches and folds and becomes indistinguishable from a one-dimensional idealized material line. The variation along a material line of the total stretching experienced by fluid elements is examined, and it is found that it can be decomposed into an overall time-dependent factor, constant along the line, and a smooth time-independent deviation. The stretching is related by a power law to the curvature of the line near sharp bends. This is confirmed numerically and motivated by a simple model. A conservation law for Lyapunov exponents explains deviations from a power-law.

I.   INTRODUCTION

The literature on the deformation of fluid elements in chaotic and turbulent flows is immense. Mainly the focus has been on the Lyapunov exponents, which characterize the exponential rate of separation of neighboring trajectories, and thus also represent the rate of stretching of fluid elements. For instance, the distribution of Lyapunov exponents has been used to characterize the diffusive decay of variance of an advected scalar [1–6], because in incompressible flows the stretching of fluid elements has an associated contraction and thus serves to amplify gradients, thus enhancing the efficiency of diffusion.

Much less attention has been paid the evolution of curvature in chaotic and turbulent flows. The curvature represents a higher-order deformation of fluid elements than stretching. To leading order, one can think of the stretching as deforming an initially spherical fluid element into an ellipsoid; the curvature then represents a bending of the axes of the ellipsoid. Since stretching tends to occur along a dominant direction, so the effect of curvature is most easily observed along that dominant direction of stretching. Mathematically, the stretching depends on first derivatives of the velocity field (essentially the local strain), whereas curvature depends on its first and second derivatives.

It has been observed that the magnitude of stretching and of curvature are anticorrelated in a flow [7]: wherever the flow experiences large amounts of stretching the fluid elements (and hence material lines) tend to be straight, and vice-versa. Intuitively, one can see that this is a result of the competing effects of curvature and stretching: the flow can pull on a material line or bend it, but the effects are orthogonal—stretching is the result of a pull along the material line, whereas curvature arises from perpendicular deformations. This provides a

[*]Electronic address: `jeanluc@mailaps.org`
[†]Present address: Department of Mathematics, Imperial College London, SW7 2AZ, United Kingdom.

motivation for the study of curvature in a flow, because being a purely geometrical quantity it can be measured directly from pictures of material lines (which can easily be obtained from experiments). In this manner one can get a rough estimate of regions of high and low stretching. This is a useful guide when trying to maximize the efficiency of mixing by varying the properties of the flow [8, 9].

In the present paper we explore the form of the dependence between stretching and curvature along material lines. There is a $-1/3$ power-law relation between the magnitude of stretching and curvature along sharp bends of material lines advected by a flow. We present evidence for this based on numerical experiments. We then explain the $-1/3$ power law using two models. The first is based on a single sharp bend in a material line where only the shape of the bend is taken into account; it has the advantage of being straightforward and intuitive, but does not account for the range of features observed. The second model uses a foliation of bends, to correct the deficiency of the first model of treating material lines as isolated objects in the flow. We make use of a local "conservation law" for Lyapunov exponents that allows a more complete description of the relationship between curvature and stretching for the foliation of bends. In particular, the conservation law predicts a dependence on the shape of neighboring material lines near a particular bend.

II. STRETCHING OF A MATERIAL LINE

We first discuss the kinematics of stretching of a material line advected by a flow $\boldsymbol{x} = \Phi(t, t_0; \boldsymbol{a})$ in an n-dimensional space. Here $\boldsymbol{x}$ is the position at time t (the Eulerian coordinate) of a fluid element that was originally at $\boldsymbol{a}$ at time t_0 (the Lagrangian coordinate). The flow Φ is typically the result of the integration of a velocity field $\boldsymbol{v}(\boldsymbol{x}, t)$, but it could also be given by a map.

A vector $\mathbf{w}_0$ is transformed to a vector $\mathbf{w}$ at time t by the relation

$$w^i(\boldsymbol{x}, t) = M^i{}_q w_0^q(\boldsymbol{a}, t_0), \qquad M^i{}_q = [\mathbb{M}]^i{}_q := \frac{\partial \Phi^i}{\partial a^q}(t, t_0; \boldsymbol{a}), \tag{1}$$

where repeated indices are summed; $\mathbb{M}$ is known as the tangent mapping of the flow. Because we are interested in the state of material lines in the Eulerian ($\boldsymbol{x}$) frame, we wish to hold $\boldsymbol{x}$ constant and integrate backward in time to obtain $\boldsymbol{a} = \Phi^{-1}(t, t_0; \boldsymbol{x})$ (if Φ is a map we iterate its inverse). We thus rewrite the tangent mapping as a function of $\boldsymbol{x}$,

$$\mathbb{M} = \frac{\partial \Phi}{\partial \boldsymbol{a}}(t, t_0; \Phi^{-1}(t, t_0; \boldsymbol{x})) = \left\{ \frac{\partial \Phi^{-1}}{\partial \boldsymbol{x}}(t, t_0; \boldsymbol{x}) \right\}^{-1}, \tag{2}$$

which can easily be verified by differentiating the identity $\Phi(t, t_0; \Phi^{-1}(t, t_0; \boldsymbol{x})) = \boldsymbol{x}$ with respect to $\boldsymbol{x}$. The matrix $\mathbb{M}$ is obtained directly from integrating

$$\frac{\partial}{\partial t_0} \mathbb{M} = -\mathbb{M} \cdot (\nabla \boldsymbol{v})^T, \qquad \mathbb{M}(t_0 = t) = I, \tag{3}$$

as $t_0 \to -\infty$; here $\nabla \boldsymbol{v}$ is evaluated at $\boldsymbol{a} = \Phi^{-1}(t, t_0; \boldsymbol{x})$. In practice, there are more accurate numerical methods available, based on matrix decomposition techniques [10–12].

The stretching of vectors as they are advected by the flow is expressed in the Eulerian frame by the left Cauchy–Green tensor [13],

$$g^{ij} := \sum_{q=1}^{n} M^i{}_q M^j{}_q. \tag{4}$$

Being a symmetric positive-definite matrix, the Cauchy–Green tensor g admits n real positive eigenvalues $\Lambda_\mu^2(\boldsymbol{x}, t, t_0)$ with corresponding orthonormal eigenvectors $\hat{\mathbf{e}}_\mu(\boldsymbol{x}, t, t_0)$. We assume that the eigenvalues are nondegenerate (at least for large $t-t_0$), and without loss of generality order them such that $\Lambda_1 > \Lambda_2 > \ldots > \Lambda_n$. The Λ_μ's are called the *coefficients of expansion*, and their exponential growth rates

$$\lambda_\mu := \frac{1}{t - t_0} \, \log \Lambda_\mu \tag{5}$$

are known as the finite-time Lyapunov exponents. The theorem of Oseledec [14] asserts that for ergodic measure-preserving systems the limit as $t \to \infty$ (or in our case $t_0 \to -\infty$) exists for almost all initial conditions (or in our case the final condition $\boldsymbol{x}$ at t, held fixed). The positivity of the largest Lyapunov exponent is the usual criterion for the presence of chaos. Because the eigenvalue of largest stretching plays an important role in our development, we often write Λ_u and $\hat{\mathbf{u}}$ for Λ_1 and $\hat{\mathbf{e}}_1$, where the letter u stands for "unstable". Note that we shall not assume that λ_u has converged, only that it is positive "most of the time," in the sense that Λ_1 is exponentially large for large $t - t_0$. Thus our treatment is valid even for aperiodic flows, where the Lyapunov exponents are not guaranteed to converge.

The eigenvector $\hat{\mathbf{u}}$ is the direction along which a fluid element has on average experienced the most stretching throughout its history; this direction converges exponentially to an asymptotic direction $\hat{\mathbf{u}}^\infty(\boldsymbol{x}, t)$ as $t_0 \to -\infty$ [10–12]. We can integrate this vector field,

$$\frac{\partial \boldsymbol{x}_\mathrm{u}}{\partial s} = \hat{\mathbf{u}}^\infty(\boldsymbol{x}_\mathrm{u}(s, t), t), \qquad \hat{\mathbf{u}}^\infty(\boldsymbol{x}_\mathrm{u}(0, t), t) = \hat{\mathbf{u}}^\infty(\overline{\boldsymbol{x}}, t), \tag{6}$$

to yield a curve $\boldsymbol{x}_\mathrm{u}(s, t)$ through $\overline{\boldsymbol{x}}$. This (infinite) curve is known as the *global unstable manifold* through $\overline{\boldsymbol{x}}$, and is parametrized by the arc length s along the curve from $\overline{\boldsymbol{x}}$. It corresponds to the unstable manifold of a hyperbolic orbit and converges to that orbit as $t_0 \to -\infty$. In a given chaotic region, all global unstable manifolds are equivalent to each other [15]; this equivalence class of unstable manifolds is called the *unstable foliation*. We will think of the representative point $\overline{\boldsymbol{x}}$ as labeling a particular unstable manifold.

Now consider a material line $\mathcal{C}$ at time t, and let $\hat{\boldsymbol{\ell}}(\boldsymbol{x}, t)$ be the unit tangent to the line $\mathcal{C}$ at $\boldsymbol{x}$. It is well-known that a material line advected by a chaotic flow aligns with the unstable foliation of the flow, a phenomenon sometimes referred to as *asymptotic directionality* [15]. Intuitively, it is clear that if fluid elements are being stretched along a preferred direction then they appear to align along that direction. This means that the tangent $\hat{\boldsymbol{\ell}}$ aligns with the most unstable eigenvector $\hat{\mathbf{u}}^\infty$ of the flow as $t_0 \to -\infty$. The components of $\hat{\boldsymbol{\ell}}$ initially orthogonal to $\hat{\mathbf{u}}^\infty$ decay in proportion to their slower stretching rates as compared to Λ_u. This can be expressed as

$$\hat{\boldsymbol{\ell}}(\boldsymbol{x}, t, t_0) = \sum_{\nu=1}^{n} \frac{\Lambda_\nu}{\Lambda_\mathrm{u}} \, \sigma_\nu(\boldsymbol{a}, t, t_0) \, \hat{\mathbf{e}}_\nu^\infty(\boldsymbol{x}, t) \tag{7}$$

where the σ_ν are nonexponential functions, that is, they may grow or decay algebraically (or be identically zero) but may not do so exponentially; they are given by the initial condition of $\hat{\boldsymbol{\ell}}(\boldsymbol{x}, t_0, t_0)$. The normalization condition of $\hat{\boldsymbol{\ell}}$ implies

$$\sigma_1 = \pm \Big(1 - \sum_{\nu > 1} (\Lambda_\nu / \Lambda_\mathrm{u})^2 \, \sigma_\nu^2 \Big)^{1/2}, \tag{8}$$

where the sign ambiguity occurs because the direction of the alignment is a matter of convention. Thus $|\sigma_1| \to 1$ as $t_0 \to -\infty$, whereas the other σ_ν decay exponentially as Λ_ν/Λ_u, a consequence of the ordering and nondegeneracy assumptions for the Λ_ν's.

Let ds denote the infinitesimal element of arc length at some point on the line. To measure the relative growth of this element, we need to know its length ds_0 at an earlier time $t_0 < t$,

$$ds_0 = \left(g_{ij}^{-1}\, \hat{\ell}^i\, \hat{\ell}^j \right)^{1/2} ds. \tag{9}$$

The square-root in (9) is the Jacobian $|\partial s_0/\partial s|$, since the arc length changes by the same proportion as the length of the tangent. Inserting the tangent (7) in the expression (9) for the length element, we find

$$ds_0 = \left(\sum_\nu \frac{\Lambda_\nu^2}{\Lambda_u^2} \sigma_\nu^2 \, \Lambda_\nu^{-2} \right)^{1/2} ds = \Lambda_u^{-1} \left(\sum_\nu \sigma_\nu^2 \right)^{1/2} ds, \tag{10}$$

where we have used $g_{ij}^{-1}\, (\hat{e}_\nu^\infty)^j = \Lambda_\nu^{-2}\, (\hat{e}_\nu^\infty)^i$ from the definition of the eigenvectors. Because of the chaotic nature of the flow, $\Lambda_u = \exp(\lambda_u t)$ grows exponentially in time, with $\lambda_u(\boldsymbol{x}, t)$ the largest finite-time Lyapunov exponent. In general, then, the ratio ds/ds_0 grows exponentially with $t - t_0$, reflecting the growth of material lines as they are advected by the flow.

The local stretching of the line, ds/ds_0, varies both because of the inherent nonuniformity in infinitesimal stretching, as described by Λ_u, but also because the initial material line at t_0 is typically aligned differently with respect to the global unstable manifold at different points, as described by the σ_ν's. However, the first effect is exponential in time, whereas the second is only algebraic. We can further differentiate these temporal behaviors, as we now proceed to show.

If $t - t_0$ is moderately large then the material line has aligned with the global unstable manifold, that is, it is tangent to $\hat{\mathbf{u}}^\infty$ at every point. The relative change in Λ_u^{-1} along $\hat{\boldsymbol{\ell}}$ satisfies

$$\hat{\boldsymbol{\ell}} \cdot \nabla \log \Lambda_u^{-1} = \hat{\boldsymbol{\ell}} \cdot \nabla \log \widetilde{\Lambda}_u^{-1} + \mathrm{O}\left(\Lambda_u^{-1}, \Lambda_2/\Lambda_u \right), \qquad \text{for } |t - t_0| \gg 1, \tag{11}$$

where $\widetilde{\Lambda}_u$ depends on $\boldsymbol{x}$ and t but not on the initial time t_0. (We define $\widetilde{\Lambda}_u$ more precisely below in (13).) This asymptotic form is a consequence of the results on derivatives of finite-time Lyapunov of Ref. [12]. It is also straightforward to show that the relative change in σ_ν is

$$\hat{\boldsymbol{\ell}} \cdot \nabla \log \sigma_\nu = \mathrm{O}\left(\Lambda_u^{-1} \right), \qquad \text{for } |t - t_0| \gg 1, \tag{12}$$

consistent with the σ_ν being defined in Lagrangian coordinates, so the stretching along $\hat{\mathbf{u}}^\infty$ in Eulerian coordinates smooths out their functional dependence.

Integrating equation (11) allows us to write

$$\Lambda_u(\boldsymbol{x}, t, t_0) \simeq \Lambda_u(\overline{\boldsymbol{x}}, t, t_0)\, \widetilde{\Lambda}_u(\boldsymbol{x}, t), \qquad \text{for } |t - t_0| \gg 1, \tag{13}$$

where $\Lambda_u(\overline{\boldsymbol{x}}, t, t_0)$ is the coefficient of expansion evaluated at an arbitrary reference point $\overline{\boldsymbol{x}}$ on the manifold $\boldsymbol{x}_u(s, t)$, defined by Eq. (6). This is true as long as we are considering a line segment $\mathcal{C}(t)$ that is shorter than Λ_u, otherwise the higher-order terms in (11) cannot be neglected. The asymptotic exponential dependence of Λ_u on $t - t_0$ is entirely contained in $\Lambda_u(\overline{\boldsymbol{x}}, t, t_0)$, because $\widetilde{\Lambda}$ does not depend on t_0.

Similarly, Eq. (12) implies that the σ_ν are constant in space along $\mathcal{C}(t)$ as long as it is shorter than Λ_{u}. We can then absorb the constant $(\sum \sigma_\nu^2)^{1/2}$ into $\Lambda_{\mathrm{u}}(\overline{\boldsymbol{x}}, t, t_0)$ and rewrite (10) as

$$ds/ds_0 = \Lambda_{\mathrm{u}}(\overline{\boldsymbol{x}}, t, t_0)\, \widetilde{\Lambda}_{\mathrm{u}}(\boldsymbol{x}, t), \tag{14}$$

where $\Lambda_{\mathrm{u}}(\overline{\boldsymbol{x}}, t, t_0)$ is constant in space along the line $\mathcal{C}$.

The main result of this section is thus given by (14). In the remainder of this paper we shall examine line segments at fixed $\boldsymbol{x}$ and t, letting t_0 recede to $-\infty$. Since the segments we consider are much shorter than Λ_{u}, we find that the local stretching (coefficient of expansion) of a material line can be characterized by the deviation $\widetilde{\Lambda}_{\mathrm{u}}(\boldsymbol{x}, t)$ from the overall stretching of the line segment, $\Lambda_{\mathrm{u}}(\overline{\boldsymbol{x}}, t, t_0)$. The somewhat surprising results are that (i) the deviation $\widetilde{\Lambda}_{\mathrm{u}}(\boldsymbol{x}, t)$ is independent of t_0, and (ii) the overall stretching of the line is well-defined (*i.e.*, it is constant along the line). The rate of overall stretching of the line of course converges to the topological entropy.

We note in closing this section that there is an ambiguity in the decomposition (13): $\Lambda_{\mathrm{u}}(\overline{\boldsymbol{x}}, t, t_0)$ and $\widetilde{\Lambda}_{\mathrm{u}}(\boldsymbol{x}, t)$ are only defined up to a multiplicative function of $\overline{\boldsymbol{x}}$ and t. We resolve this by integrating (14) over $\mathcal{C}$, to find

$$L(t)/L(t_0) = \Lambda_{\mathrm{u}}(\overline{\boldsymbol{x}}, t, t_0) \left\langle \widetilde{\Lambda}_{\mathrm{u}}^{-1} \right\rangle_{\mathcal{C}(t)}^{-1}, \tag{15}$$

where $L(t)$ is the length of $\mathcal{C}(t)$ and $\langle \cdot \rangle_{\mathcal{C}(t)}$ is an average over the line $\mathcal{C}(t)$. Clearly a proper definition of the overall growth $\Lambda_{\mathrm{u}}(\overline{\boldsymbol{x}}, t, t_0)$ of the material line should be that it is equal to the growth of the length $L(t)/L(t_0)$. An appropriate choice for the definition of $\Lambda_{\mathrm{u}}(\overline{\boldsymbol{x}}, t, t_0)$ and $\widetilde{\Lambda}_{\mathrm{u}}(\boldsymbol{x}, t)$ is thus to scale them such that

$$\left\langle \widetilde{\Lambda}_{\mathrm{u}}^{-1} \right\rangle_{\mathcal{C}(t)} = 1, \tag{16}$$

which we assume to hold.

III. NUMERICAL RESULTS

In this section we present the result of numerical calculations comparing the stretching and the curvature along material lines. Because we are interested in material lines that have evolved for a long time in the flow (long compared to the inverse Lyapunov exponent), it is sufficient to compute the shape of unstable manifolds by integrating (6) starting at sample points $\boldsymbol{x}$ at time t in the fluid domain.

Two prototypical systems will be used. The first is the ubiquitous standard map,

$$x_{n+1} = x_n + y_{n+1}, \qquad y_{n+1} = y_n + (K/2\pi) \sin(2\pi x_n), \tag{17}$$

where $(x, y) \in [0, 1] \times [0, 1]$. Maps of course have the advantage that they are computationally efficient, allowing rapid verification of results. Another desirable feature of (17) is that for large K the structure of material lines advected by the map is fairly simple, as evidenced in Fig. 1(a) which has $K = 50$. The diagonal bias in the figure is due to the sweeping of the sine wave on both side of (17), which at such large K traverses the domain several times for each iteration, breaking (almost) all islands. The map is area-preserving, so that the determinant of g is $|g| = 1$.

(a)   (b)
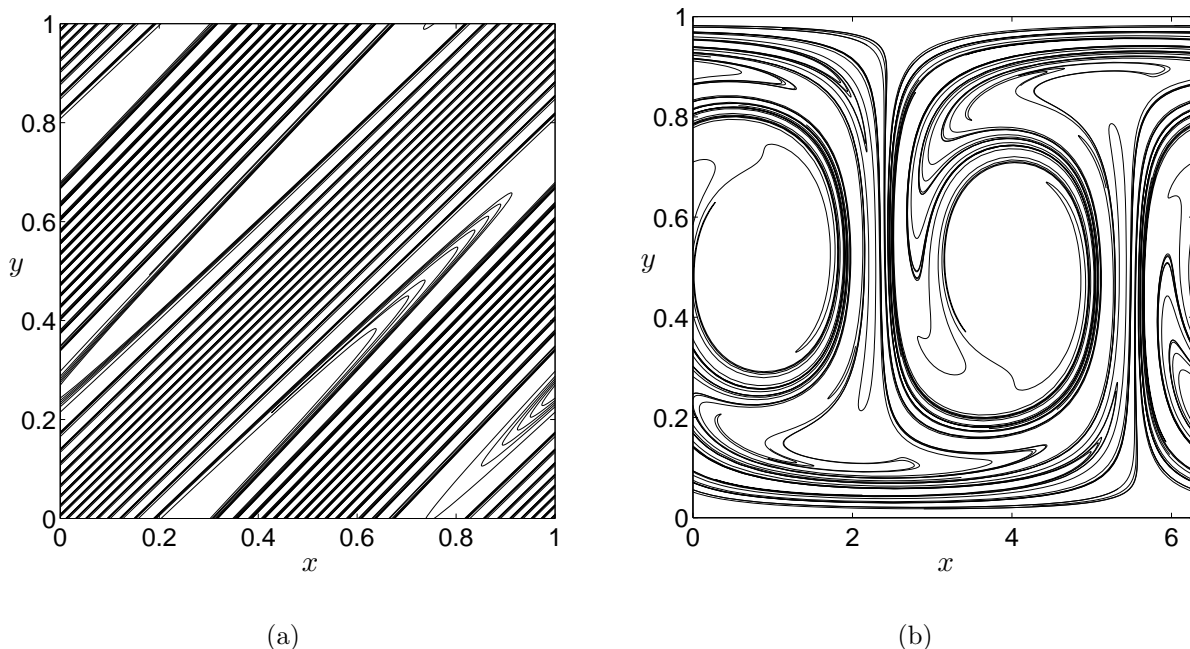
FIG. 1: Material lines advected by (a) the standard map with $K = 50$ and (b) the cellular flow
with $A = \epsilon = \omega = k = 1$.

The second system we shall use is the cellular flow of Solomon and Gollub [16], with
velocity field

$$\boldsymbol{v} := \left(-\frac{\partial\psi}{\partial y}, \frac{\partial\psi}{\partial x}\right), \qquad \psi(\boldsymbol{x}, t) := A\,k^{-1}(\sin kx + \epsilon \cos\omega t\, \cos kx)\sin^2 \pi y, \qquad (18)$$

to model an array of oscillating convection rolls, periodic in x and with rigid walls at $y = 0$
and $y = 1$. The $\sin^2 \pi y$ dependence is chosen to satisfy the rigid boundary conditions at the
walls. The velocity field is incompressible ($\nabla \cdot \boldsymbol{v} = 0$), so that $|g| = 1$. When $\omega = 0$, the flow
is steady, and the trajectories of fluid elements are nonchaotic. This is true in general of
any two-dimensional steady flow [17]. A snapshot of typical material lines advected by (18)
are shown in Fig. 1(b). Note the two large regular islands in the center.

Our interest lies in the variations of stretching and curvature along material lines. The
local stretching is given by the coefficient of expansion Λ_{u}, but since we let the material
lines evolve for some time (such that $\Lambda_{\mathrm{u}} \gg 1$) it is sufficient to consider the t_0-independent
deviation from mean stretching, $\widetilde{\Lambda}_{\mathrm{u}}$, defined in Section II. Thus, for convenience we will refer
to $\widetilde{\Lambda}_{\mathrm{u}}$ as "the stretching" even though it needs to be multiplied by an overall factor $\Lambda(\overline{\boldsymbol{x}}, t, t_0)$
to represent the total stretching a line has experienced.

Figure 2 is a plot of the stretching and curvature as they vary along a typical material line
advected by our two prototypical systems. The first thing to note is that the stretching $\widetilde{\Lambda}_{\mathrm{u}}$
is smooth along the material line (the sharp dips are well-resolved). It is known that the
finite-time Lyapunov exponents are not continuous functions of the spatial variables, but
Fig. 2 underscores that the rough variation of the exponents (and hence the stretching)
occurs perpendicular to the unstable direction. In the Lagrangian frame, holding $\boldsymbol{a}$ fixed
instead of $\boldsymbol{x}$, it is the variation along the contracting direction that is smooth [18, 19]. (The
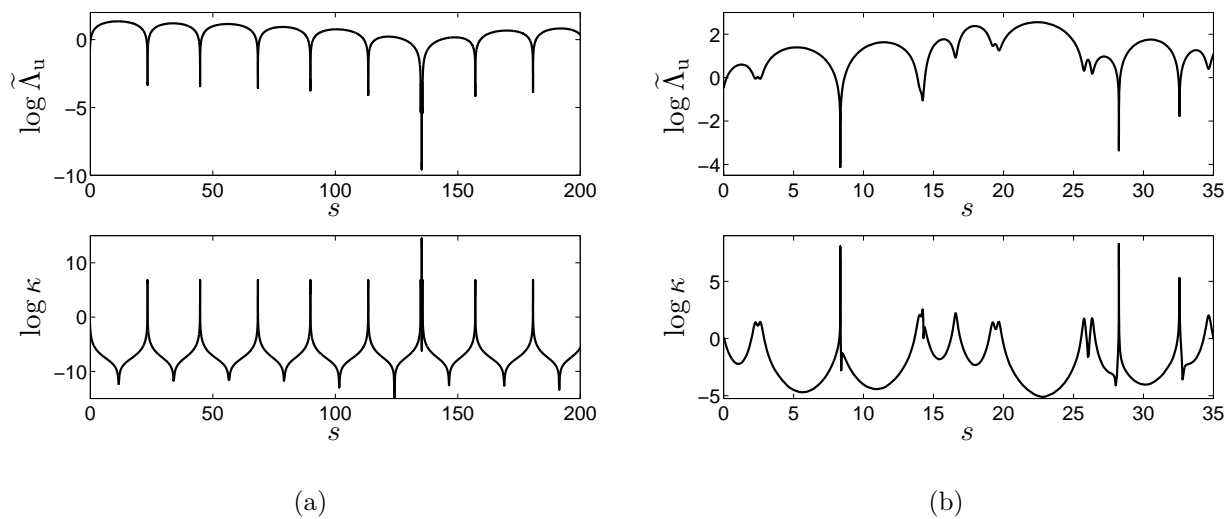
FIG. 2: The stretching, $\widetilde{\Lambda}_{\mathrm{u}}$, and the magnitude of the curvature, κ, plotted against the arc length s along a material line for (a) the standard map; and (b) the cellular flow. The parameter values are as in Fig. 1. Note the close anticorrelation between stretching and curvature.

variation of the stretching along the characteristic directions is discussed in Ref. [12].)

A second observation is that the variations in the stretching are very large, encompassing about four orders of magnitude or more in typical cases. This says that not all points in the flow are equally propitious to stretching, and that the variations can be sizeable even within a single chaotic region. Because the coefficient of expansion denotes a fluid element's history of stretching, the large variations imply that some trajectories avoid regions of significant stretching for a long time.

The third striking feature of Fig. 2 is the close anticorrelation between stretching and curvature—high curvature regions are invariably associated with relatively low stretching. This phenomenon was first observed by Drummond and Münch [7] in the context of a model turbulent flow, based on earlier work of Pope *et al.* on the curvature of fluid elements [20, 21]. This and later work on turbulence and random flows [22–25] and deterministic flows [24, 26–28] focused on the probability distribution of curvature and on comparing stretching and curvature at a point. Here we investigate how stretching and curvature vary along material lines, with the intention of gaining a better understanding of their relationship.

With this in mind it is natural to plot the stretching and curvature of Fig. 2 as a parametric (or phase) plot, that is, we plot them against each other while increasing the arc length along the line. The result is shown in Fig. 3. A power-law relation between stretching and curvature around sharp bends (large curvature) is immediately apparent, with exponent $-1/3$. This power-law behavior is especially well-realized for the standard map (Fig. 3(a)). Fig. 3(a) also shows that for the same maximum curvature, bends can have very different peak stretchings, so even though there is a power-law relationship between curvature and stretching, the peak stretching is not directly related to the peak curvature.

In a related context involving the stable manifold in the Lagrangian frame, the exponent was measured as -0.331 by Tang and Boozer [18]. In the following two sections we use two models of increasing refinement to justify an exponent of exactly $-1/3$ and illuminate the cause of the power-law relation.
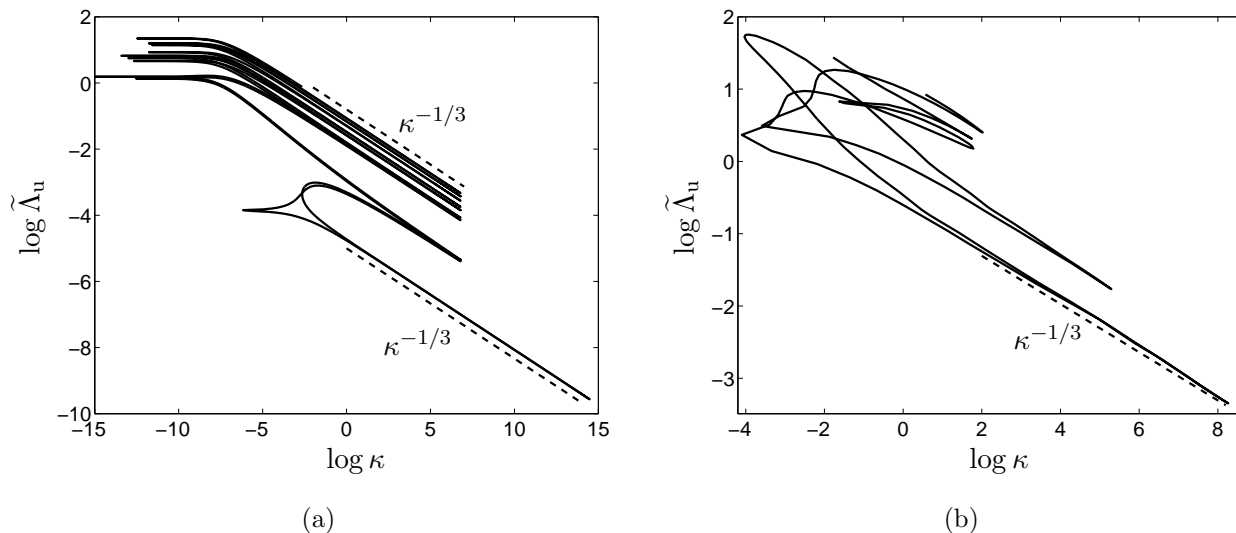
FIG. 3: Parametric plot of the stretching, $\widetilde{\Lambda}_{\mathrm{u}}$, against the magnitude of the curvature, κ, along a material line for (a) the standard map; and (b) the cellular flow. The parameter values are as in Fig. 1. For sharp bends there is a power-law relationship between the curvature and the stretching. From (a), it is clear that for the same maximum curvature, bends can have very different peak stretching factors.

IV. ANALYSIS FOR A SINGLE BEND

We propose a simple physical picture in 2D to reproduce the $\widetilde{\Lambda}_{\mathrm{u}} \sim \kappa^{-1/3}$ law around sharp bends. We refer to this picture as the "simple bend model". We examine the model in detail, and point out its advantages and failures. Its advantages are simplicity and a physically intuitive formulation. Its failures are that it refers to a specific initial configuration of the material line, and that it does not account for the deviations from the $-1/3$ law observed in Fig. 3; these shortcomings will be addressed by a more refined model in Section V.

Consider an initially straight material line of length L, as illustrated at the top of Fig. 4(a), parametrized by $(x(s), y(s)) = (s, 0)$ with $s \in [0, L]$. The material line will be stretched and folded by the flow, as in Fig. 4(a). We parametrize the shape of the fold by

$$\boldsymbol{x}(s) = (x(s), y(s)) = (\beta s, f(s)), \qquad s \in [0, L], \tag{19}$$

where f determines the shape of the bend, and β its horizontal extent. From this we can directly compute the curvature,

$$\kappa = \frac{\|\boldsymbol{x}'(s) \times \boldsymbol{x}''(s)\|}{\|\boldsymbol{x}'(s)\|^3} = \beta \, |f''(s)| \, \|\boldsymbol{x}'(s)\|^{-3}. \tag{20}$$

But $\|\boldsymbol{x}'(s)\|$ is a measure of $\widetilde{\Lambda}_{\mathrm{u}}$, the relative local stretching of the material line [28]. Hence, if the variation in $|f''(s)|$ can be neglected, Eq. (20) gives the desired power-law relationship between curvature and stretching. That $|f''(s)|$ can be neglected is a consequence of the sharpness of the bend: a Taylor series expansion of f (in a rotated and translated coordinate system)

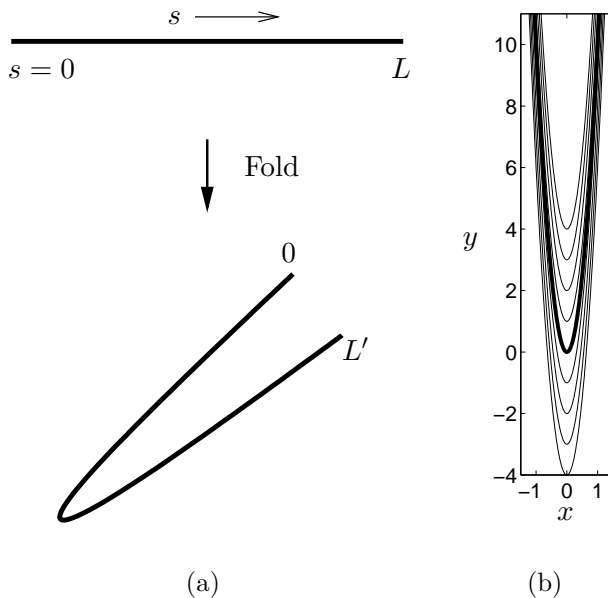$$f(s) = \tfrac{1}{2}\kappa_0 \, s^2 + \mathrm{O}(s^3) \tag{21}$$

FIG. 4: (a) Schematic representation of a material line folded by a flow. (b) A foliation of bends.

will be dominated by the quadratic term near the tip of the bend: the cubic and other odd terms cannot dominate, otherwise the profile would not resemble a sharp bend. While it is possible that quartic or higher-order terms are important in characterizing the shape of a given bend, we assume that there is nothing special about this particular bend so that the quadratic term dominates (in principle many shapes of bends will occur in a chaotic flow). This will always be true if we are near enough the tip. The coefficient κ_0 is large and gives the curvature at the tip of the bend.

It is encouraging that such a straightforward physical picture reproduces the salient features of stretching and folding in a chaotic flow. But there are problems with the simple bend model. First, it requires a consideration of the initial shape of the material line. In a chaotic flow, the $-1/3$ law is observed for arbitrary initial conditions. The second problem is that deviations from the strict $-1/3$ law are not of the form predicted by the model. In Fig. 3, some of the bends appear "fat", that is, the maxima of stretching and curvature do not exactly coincide. The only deviations allowed in the simple bend model arise from a non-quadratic bend profile. But the bends that exhibit deviations from the law in Fig. 3 have a profile that is essentially quadratic near the tip.

We resolve this discrepancy in Section V by allowing the bend to be surrounded by a continuum (a *foliation*) of other bends and using a conservation law for Lyapunov exponents.

V.   A CONSERVATION LAW FOR LYAPUNOV EXPONENTS

The failures of the simple bend model in Section IV lies in the material lines not being isolated objects in the fluid: they are surrounded by a continuum of other material lines. Figure 1(a) shows a material line that has been advected by the standard map, for a large value of the control parameter K (by "advection" in the context of a map we simply mean iterating an initial distribution). At these highly chaotic values of K, the material line

exhibits a surprising degree of regularity. Indeed, the visible folds (there are also tiny bends too small to see) resemble a nested set of the simple bend we discussed in Section IV. This suggests extending the model to treat a *foliation* of curves, as shown in Fig. 4(b), where the thick curve is the bend under consideration (the nominal bend) and the others are neighboring bends (not necessarily identical to the nominal bend).

The tangent $\boldsymbol{\ell}(x, y)$ near the thick bend $y = f(x)$ of Fig. 4(b) can be written

$$\boldsymbol{\ell}(x, y) = (1, \, f'(x) + h(x, y - f(x))), \qquad h(x, 0) = 0, \tag{22}$$

with the unit tangent $\hat{\boldsymbol{\ell}} = \boldsymbol{\ell}/\|\boldsymbol{\ell}\|$. Thus, when evaluated on the curve $y = f(x)$, we have $\boldsymbol{\ell} = (1, \, f'(x))$ and we recover the tangent to the curve. The function h represents changes in the tangent to the bends as we move off our nominal bend $y = f(x)$. Both f and h are left unspecified for now.

To analyze the variation of stretching on the nominal bend, it is sufficient to know how Λ_u varies along $\hat{\mathbf{u}}^\infty$, the characteristic direction of stretching of fluid elements. This is because material lines can be assumed to be aligned with the unstable foliation, as described in Section II. We will obtain this variation from the formula

$$|g|^{1/2}\nabla \cdot \left(|g|^{-1/2}\, \hat{\mathbf{u}}\right) + \hat{\mathbf{u}} \cdot \nabla \log \Lambda_u \sim \max(\Lambda_u^{-1}, \Lambda_2/\Lambda_u) \longrightarrow 0, \tag{23}$$

which holds for for large $t - t_0$, when we can replace $\hat{\mathbf{u}}$ by $\hat{\mathbf{u}}^\infty$. Here $|g|$ is the determinant of g. This is a "constraint" on the variation of Λ_u along the unstable manifold in chaotic flows and maps. It was derived for arbitrary dimension in Ref. [12]. It traces its origins in an analogous relation for the stable manifold in Lagrangian coordinates, obtained using methods from differential geometry [18, 19]. A similar result was obtained in the 2D incompressible case in Ref. [15], where it was used to derive an invariant measure to characterize intermaterial contact area. In dimensions greater than two, the characteristic directions and finite-time Lyapunov exponents associated with a chaotic flow must obey other constraints [12], but (23) is the only one we will use here.

Assuming that the material line has evolved long enough that the constraint (23) is satisfied to any desired accuracy, and assuming that the flow is incompressible, we rewrite the constraint as

$$\frac{\partial}{\partial s} \log \Lambda_u + \nabla \cdot \hat{\mathbf{u}}^\infty = 0, \tag{24}$$

where s is the arc length along the material line (*i.e.*, the unstable manifold). Actually, incompressibility is sufficient to have (24), but it is not necessary as any flow with $|g|$ constant in space will satisfy (24). This is the case, for instance, in the Lorenz equations, where $\nabla \cdot \boldsymbol{v} = \text{constant}$.

Equation (24) is a conservation law for the largest Lyapunov exponent λ_u: if neighboring unstable manifolds converge (diverge), then the largest finite-time Lyapunov exponent increases (decreases). Physically, the conservation law (24) can be justified by thinking of converging unstable manifolds (or equivalently the material line) as "squeezing" fluid elements, thereby also stretching them if the flow is incompressible. In 3D the unstable manifolds squeezes fluid elements by the same amount because they must preferentially stretch along the unstable manifold (the stretching that can occur along the intermediate direction $\hat{\mathbf{e}}_2$ is negligible, because we assumed nondegenerate Λ_σ's so that $\Lambda_u \gg \Lambda_2$ after some time).

Returning to our model of a foliation of bends, the divergence of $\hat{\mathbf{u}}^\infty$ evaluated on $y = f(x)$ is easily computed,

$$\nabla \cdot \hat{\mathbf{u}}^\infty \simeq \nabla \cdot \hat{\boldsymbol{\ell}} = -\frac{f'(f'' + h_1(x, 0))}{(1 + f'^2)^{3/2}} + \frac{h_2(x, 0)}{(1 + f'^2)^{1/2}}, \tag{25}$$

since the tangent (22) to the curve is aligned with the unstable manifold. The subscripts 1 and 2 on h denote differentiation with respect to its first and second arguments. We may think of $h_1(x, 0)$ as the variation in the tangent $\hat{\boldsymbol{\ell}}$ along x, and of $h_2(x, 0)$ as the variation along y, both parametrized by x, where the x–y coordinates are defined in Fig. 4(b).

We evaluate the other term of the constraint (24) on $y = f(x)$,

$$\frac{\partial}{\partial s} \log \Lambda_{\mathrm{u}} = \hat{\mathbf{u}}^\infty \cdot \nabla \log \Lambda_{\mathrm{u}} = \frac{1}{(1 + f'^2)^{1/2}} \frac{d}{dx} \log \Lambda_{\mathrm{u}}, \tag{26}$$

so that from (23), (25), and (26), we find

$$\frac{d}{dx} \log \Lambda_{\mathrm{u}} = \frac{f'(f'' + h_2(x, 0))}{1 + f'^2} - h_1(x, 0). \tag{27}$$

This can be integrated to yield

$$\Lambda_{\mathrm{u}} = c \, (1 + f'^2)^{1/2} \exp \left(\int \frac{f'(x) \, h_1(x)}{1 + f'^2} \, \mathrm{d}x - \int h_2(x, 0) \, \mathrm{d}x \right), \tag{28}$$

where c is constant in space along the material line but depends on time (it contains the exponential growth of Λ_{u}). The integrals in (28) are indefinite.

First we show that we recover the result of Section IV in the limit $h_1 = h_2 = 0$ (a uniform foliation of bends). To exhibit the relationship between stretching and curvature, we use the expression

$$\kappa(x) = \frac{|f''(x)|}{(1 + f'(x)^2)^{3/2}} \tag{29}$$

for the magnitude $\kappa(x)$ of the curvature, and obtain from (28)

$$\Lambda_{\mathrm{u}} = c \, |f''(x)|^{1/3} \, \kappa^{-1/3} \tag{30}$$

after setting $h_1 = h_2 = 0$. Equation (30) agrees with (20), with $c^3 = \beta^{-1}$. However, Eq. (30) has been derived with no assumption as to the initial shape of the material line.

Now we look for deviations from the $-1/3$ law. The integrals in (28) depend on the exact form of f and $h_{1,2}(x, 0)$. But as a lowest-order approximation, near the tip of the bend (at $x = 0$) we may assume that f is quadratic and $h_{1,2}(x, 0) =: h_{1,2} = $ constant, the first nonzero terms in a power series. The resulting stretching is

$$\Lambda_{\mathrm{u}} = c \left(1 + f'^2 \right)^{\frac{1}{2} + (h_1/2\kappa_0)} \exp \left(-h_2 \, x \right), \tag{31}$$

which may be rewritten in terms of the curvature $\kappa(x)$ using (29),

$$\Lambda_{\mathrm{u}} = c \, \kappa^{-\frac{1}{3} - (h_1/3\kappa_0)} \exp \left[\pm (h_2/\kappa_0) \left((\kappa/\kappa_0)^{-2/3} - 1 \right) \right]. \tag{32}$$
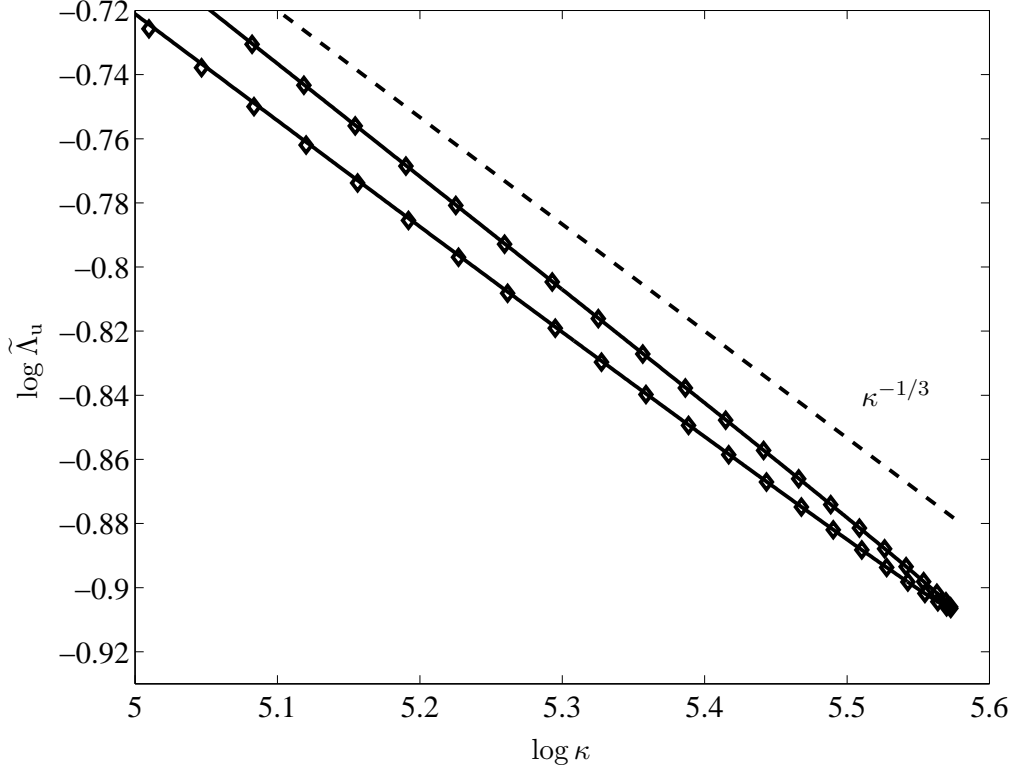
FIG. 5: Deviation from the $-1/3$ law due to nonuniformity of bends. The solid line is a fit using formula (32), and the diamonds are numerical data. The parameters used are $h_1/\kappa_0 = -0.01$, $h_2/\kappa_0 = 0.015$, where h_1 controls the deviation from the $-1/3$ law and h_2 the multi-valuedness of $\widetilde{\Lambda}$.

Thus, h_1 appears as a deviation to the exponent of the $-1/3$ law, while h_2 gives an exponential, multi-valued correction (due to the $\pm$ sign). For sharp bends, $\kappa_0 \gg 1$, so that the corrections due to h are not visible. In Fig. 5 we show a bend where the corrections are more important ($h_1/\kappa_0 = -0.01$, $h_2/\kappa_0 = 0.015$): the solid line shows that the fit of (32) to the numerical solution is very good near the tip, where we expect it to be valid.

There are several sources of deviation from the $-1/3$ law. The first is from the shape of the bend, as represented by the cubic and higher-order terms in $f(x)$. The second is in the variation of the tangent vector field (22), that is, the shape of the neighboring bends, as embodied by the function h in (22). In 3D, the variation in z (the direction perpendicular to the plane of the bend) must also be taken into account, but we do not do so here. What our analysis shows is that the simplest configuration—a uniform foliation of bends—captures the power-law behavior perfectly. The leading-order corrections are predominantly due to the function h, and not to the higher-order terms of f, at least near the tip of the bend. The reason for this is that the h terms enter (31) at lowest order in x.

Numerical investigation indicates that the $-1/3$ law often holds in 3D around sharp bends, but not always—possibly a signature of torsion (the bend is no longer planar). A complete 3D description would have to take into account possible torsion in the material lines and will be the focus of future research.

If the flow is compressible, then a simple modification of (30) starting from (23) gives

$$\Lambda_{\mathrm{u}} = c\,|g|^{1/2}\,|f''(x)|^{1/3}\,\kappa^{-1/3}\,, \tag{33}$$

where we have assumed $|g|$ depends only on x. The $-1/3$ law will thus not be affected by compressibility as long as the variations in $|g|$ are unimportant around sharp bends, which is usually the case because of the localized nature of the bends.

We may consider instead of bends a foliation of horizontal lines, so that $f'(x) \equiv 0$. Then we conclude from (28) that $\Lambda_{\mathrm{u}} = c$, for $h_2(x, 0) = 0$. Such a foliation corresponds to a region of vanishing curvature, and the constant stretching is reflected in Fig. 3(a) (upper-left portion of the plot). The cellular flow, Fig. 3(b), does not exhibit the constancy of Λ_{u} in regions of low curvature, indicating that in this less idealized situation the variation of the vector field $\hat{\mathbf{u}}^{\infty}$ perpendicular to itself cannot be neglected.

VI.   CONCLUSION

Though stretching of fluid elements is more directly relevant to physical problems such as mixing, understanding the kinematics of curvature is also important. A compelling reason is that, unlike stretching, curvature is directly measurable from simple visualization experiments, being a purely geometrical quantity. Stretching and curvature are not independent, and it is hoped that techniques such as those described herein can be used to relate their distribution. For instance, the $-1/3$ law suggests that low values of stretching are closely correlated to high curvature regions in a universal manner, and thus the corresponding tail of the two distributions can have similar properties. There is some indication that this is the case, and future work will address such statistical correlations.

Acknowledgments

[1] R. T. Pierrehumbert, "Large-scale horizontal mixing in planetary atmospheres," Phys. Fluids A **3**, 1250 (1991).

[2] T. M. Antonsen, Jr. and E. Ott, "Multifractal power spectra of passive scalars convected by chaotic fluid flows," Phys. Rev. A **44**, 851 (1991).

[3] M. Chertkov, G. Falkovich, I. Kolokolov, and V. Lebedev, "Statistics of a passive scalar advected by a large-scale two-dimensional velocity field: Analytic solution," Phys. Rev. E **51**, 5609 (1995).

[4] T. M. Antonsen, Jr., Z. Fan, E. Ott, and E. Garcia-Lopez, "The role of chaotic orbits in the determination of power spectra," Phys. Fluids **8**, 3094 (1996).

[5] D. T. Son, "Turbulent decay of a passive scalar in the Batchelor limit: Exact results from a quantum-mechanical approach," Phys. Rev. E **59**, R3811 (1999).

[6] E. Balkovsky and A. Fouxon, "Universal long-time properties of Lagrangian statistics in the Batchelor regime and their application to the passive scalar problem," Phys. Rev. E **60**, 4164 (1999).

[7] I. T. Drummond and W. Münch, "Distortion of line and surface elements in model turbulent flows," J. Fluid Mech. **225**, 529 (1991).

[8] D. M. Hobbs and F. J. Muzzio, "Optimization of a static mixer using dynamical systems techniques," Chem. Eng. Sci. **53**, 3199 (1998).

[9] X. Z. Tang and A. H. Boozer, "Design criteria of a chemical reactor based on a chaotic flow," Chaos **9**, 183 (1999).

[10] J. M. Greene and J. S. Kim, "The calculation of Lyapunov spectra," Physica D **24**, 213 (1987).

[11] I. Goldhirsch, P. Sulem, and S. A. Orszag, "Stability and Lyapunov stability of dynamical systems: A differential approach and a numerical method," Physica D **27**, 311 (1987).

[12] J.-L. Thiffeault, "Derivatives and constraints in chaotic flows: Asymptotic behaviour and a numerical method," Physica D **172**, 139 (2002).

[13] J. M. Ottino, *The Kinematics of Mixing: Stretching, Chaos, and Transport* (Cambridge University Press, Cambridge, U.K., 1989).

[14] V. I. Oseledec, "A multiplicative theorem: Lyapunov characteristic numbers for dynamical systems," Trans. Moscow Math. Soc. **19**, 197 (1968).

[15] M. Giona and A. Adrover, "Nonuniform stationary measure of the invariant unstable foliation in Hamiltonian and fluid mixing systems," Phys. Rev. Lett. **81**, 3864 (1998).

[16] T. H. Solomon and J. P. Gollub, "Chaotic particle transport in time-dependent Rayleigh–Bénard convection," Phys. Rev. A **38**, 6280 (1988).

[17] J.-P. Eckmann and D. Ruelle, "Ergodic theory of chaos and strange attractors," Rev. Mod. Phys. **57**, 617 (1985).

[18] X. Z. Tang and A. H. Boozer, "Finite time Lyapunov exponent and advection-diffusion equation," Physica D **95**, 283 (1996).

[19] J.-L. Thiffeault and A. H. Boozer, "Geometrical constraints on finite-time Lyapunov exponents in two and three dimensions," Chaos **11**, 16 (2001).

[20] S. B. Pope, "The evolution of surfaces in turbulence," Int. J. Engng Sci. **26**, 445 (1988).

[21] S. B. Pope, P. K. Yeung, and S. S. Girimaji, "The curvature of material surfaces in isotropic turbulence," Phys. Fluids A **1**, 2010 (1989).

[22] T. Ishihara and Y. Kaneda, "Stretching and distortion of material line elements in two-dimensional turbulence," J. Phys. Soc. Japan **61**, 3547 (1992).

[23] I. T. Drummond, "Stretching and bending of line elements in random flows," J. Fluid Mech. **252**, 479 (1993).

[24] M. Liu and F. J. Muzzio, "The curvature of material lines in chaotic cavity flows," Phys. Fluids **8**, 75 (1996).

[25] A. Schekochihin, S. Cowley, J. Maron, and L. Malyshkin, "Structure of small-scale magnetic fields in the kinematic dynamo theory," Phys. Rev. E **65**, 016305 (2002).

[26] D. M. Hobbs, M. M. Alvarez, and F. J. Muzzio, "Mixing in globally chaotic flows: A self-similar process," Fractals **5**, 395 (1997).

[27] D. M. Hobbs and F. J. Muzzio, "The curvature of material lines in a three-dimensional chaotic flow," Phys. Fluids **10**, 1942 (1998).

[28] S. Cerbelli, J. M. Zalc, and F. J. Muzzio, "The evolution of material field lines curvature in deterministic chaotic flows," Chem. Eng. Sci. **55**, 363 (2000).